Front. Chem. Sci. Eng. 2020, 14(4): 522–533
https://doi.org/10.1007/s11705-019-1822-3

RESEARCH ARTICLE

Preparation and investigation of Pd doped Cu catalysts for selective hydrogenation of acetylene

Xinxiang Cao[1,2,3], Tengteng Lyu[1], Wentao Xie[1], Arash Mirjalili[1], Adelaide Bradicich[1], Ricky Huitema[1], Ben W.-L. Jang (✉)[1], Jong K. Keum[4], Karren More[4], Changjun Liu[3], Xiaoliang Yan[5]

1 Department of Chemistry, Texas A&M University-Commerce, Commerce, TX 75429-3011, USA
2 Laboratory for Development & Application of Cold Plasma Technology, College of Chemistry and Chemical Engineering, Luoyang Normal University, Luoyang 471022, China
3 Collaborative Innovation Center of Chemical Science and Engineering, School of Chemical Engineering and Technology, Tianjin University, Tianjin 300072, China
4 Center for Nanophase Materials Sciences and Chemical Science Division, Oak Ridge National Laboratory, Oak Ridge, TN 37831, USA
5 College of Chemistry and Chemical Engineering, Taiyuan University of Technology, Taiyuan 030024, China

Abstract A series of PdCu bimetallic catalysts with low Cu and Pd loadings and different Cu: Pd atomic ratios were prepared by conventionally sequential impregnation (CSI) and modified sequential impregnation (MSI) of Cu and Pd for selective hydrogenation of acetylene. Characterization indicates that the supported copper (II) nitrate in the PdCu bimetallic catalysts prepared by MSI can be directly reduced to Cu metal particles due to the hydrogen spillover from Pd to $Cu(NO_3)_2$ crystals. In addition, for the catalysts prepared by MSI, Pd atoms can form PdCu alloy on the surface of metal particles, however, for the catalysts prepared by CSI, Pd tends to migrate and exist below the surface layer of Cu. Reaction results indicate that compared with CSI, the MSI method enables samples to possess preferable stability as well as comparable reaction activity. This should be due to the MSI method in favor of the formation of PdCu alloy on the surface of metal particles. Moreover, even Pd loading is super low, < 0.045 wt-% in this study, by through adjusting Cu loading to an appropriate value, attractive reactivity and selectivity still can be achieved.

Keywords copper, palladium, catalysts, acetylene, selective hydrogenation

1 Introduction

Ethylene as the feedstock of polyethylene production is usually obtained from steam thermal cracking of naphtha, during which acetylene is inevitably produced. Since trace amount of acetylene, even ppm level, can stoichiometrically poison the polymerization catalyst, the selective hydrogenation of acetylene to ethylene in excess ethylene is a crucial industrial process of the polyethylene industry [1–3].

Up to now, supported palladium is still the preferred catalyst used for selective hydrogenation of acetylene to ethylene owning to its high catalytic activity. However, Pd does not inherently offer good ethylene selectivity due to Pd ensemble size and the role of carbide/hydride phases [4]. To overcome the shortcoming of Pd catalysts, various approaches have been pursued, including the use of a second metal, such as Au, Ag, Ga, Zn, Sn, In, Pb, Co and Cu to dilute Pd ensembles [3–10], and the use of organic S, N or P as modifiers to pre-adsorb onto catalyst surface to partially cover Pd active sites, etc. [11–13]. Among these second metals, Cu has been receiving more attention recently. One reason is that Cu has a much lower cost and readily alloys with Pd. The other reason is the special property of copper. DFT and experimental studies have revealed that dissociated hydrogen readily spilled over from Pd sites onto Cu, and Cu could be activated by neighboring Pd, and thus the performance of PdCu bimetallic catalysts could be improved dramatically [14–17]. Therefore, besides the Pd sites, this activated Cu would also act as active sites for selective hydrogenation of acetylene at relatively low temperatures. This special synergy property differs from other metal promoters and makes the Pd-Cu catalyst system a potentially effective approach to significantly improve its catalytic performance for selective hydrogenation reactions.

Received October 8, 2018; accepted January 30, 2019

E-mail: Ben.Jang@tamuc.edu

Based on the literature [4,18,19], preparation methodologies significantly affect the performance of PdCu bimetallic catalysts. For instance, Pd doped Cu catalysts have been prepared by McCue and co-workers [4] with co-impregnation, sequential impregnation, and a colloidal approach. Reaction results showed that with the same Cu:Pd ratio and under the same reaction condition, the sample prepared by colloidal approach shown the poorest conversion, while, the sample made by sequential impregnation possessed the best selectivity. Cao et al. [18] have prepared a series of copper-rich PdCu/γ-Al_2O_3 catalysts by galvanic replacement, co-impregnation, and sequential impregnation. Besides the differences in selectivity and conversion, it was found that the catalyst prepared by sequential incipient wetness impregnation (IWI) had the best stability among all the resultant catalysts. Liu and co-workers [19] have reported two bimetallic PdCu catalysts containing only small amounts of Pd prepared by conventional impregnation and modified co-precipitation. Reaction results demonstrated that the sample prepared by the modified co-precipitation exhibited higher activity and selectivity than the one made by conventional impregnation. Moreover, according to the literature [20,21], catalysts undergoing low-temperature treatment instead of thermal calcination often possess some unique properties. Supported palladium with 300–500 ppm loading is commercially used for the selective hydrogenation of acetylene in excess ethylene. Moreover, due to rarity and the high cost of palladium, reducing its consumption as much as possible is also a sensible choice for Pd-based catalysts preparation. Given these, a series of PdCu bimetallic catalysts with low Cu and Pd loadings were prepared by conventionally sequential impregnation (CSI) and modified sequential impregnation (MSI), and their catalytic performance for selective hydrogenation of acetylene was compared in this study. The reduction behavior of the as-prepared fresh Cu and Pd doped Cu catalysts was characterized by H_2-TPR and *in situ* XRD. The structural evolution was investigated via H_2-TPR, *in situ* diffuse reflectance infrared Fourier transform spectroscopy (DRIFTs) of CO and HAADF-STEM-EDS.

2 Materials and methods

2.1 Catalyst preparation

Gamma alumina and palladium (II) nitrate hydrate were purchased from Alfa Aesar and copper (II) nitrate hemi (pentahydrate) from Sigma-Aldrich. The gamma alumina pellets with 1/8 diameter (surface area: 250 $m^2 \cdot g^{-1}$, pore volume: 1.14 $cm^3 \cdot g^{-1}$) were ground and sieved to 30–40 mesh followed by calcination at 450°C for 2 h. The γ-Al_2O_3 supported Pd, and Cu catalysts were prepared by IWI from an aqueous solution of $Cu(NO_3)_2$ and $Pd(NO_3)_2$ respectively. Thereafter, the samples were dried at 110°C for 12 h followed by calcination at 400°C for 3 h. The resultant samples were designated as Pd_x-cal, and Cu_y-cal, where "*x* wt-%" and "*y* wt-%" refer to the nominal loading of Pd and Cu, respectively, and "cal" represents calcination process. The Pd doped Cu catalysts, Pd_xCu_y-cal, were obtained by CSI. Briefly, Cu_y-cal was prepared as described above, and then further impregnated with palladium nitrate solution followed by drying and calcination as mentioned above also. Cu_y-vac was prepared by the impregnation of γ-Al_2O_3 by $Cu(NO_3)_2$ solution followed by drying at room temperature and pressure for 12 h and then further drying at room temperature under vacuum for another 12 h. Pd_xCu_y-vac was prepared by further impregnation of Cu_y-vac with palladium nitrate solution followed by drying steps as of Cu_y-vac. "vac" in Cu_y-vac and Pd_xCu_y-vac represents drying at room temperature under vacuum. In contrast, the preparation method for Pd_xCu_y-vac was termed as MSI in this study. The main particularity of MSI is no high-temperature calcination steps after impregnation processes.

2.2 Catalyst characterizations

The actual metal loadings of samples were determined by an atomic absorption spectrophotometer (AAS) (Shimadzu AA-6300).

Hydrogen temperature-programmed reduction (H_2-TPR) tests were conducted on an AMI-200 automated system (Altamira Instruments). A certain amount of fresh sample was reduced in 30 vol-% H_2/Ar at the flow rate of 30 $cm^3 \cdot min^{-1}$ by ramping from 25°C to 400°C at 10°C·min^{-1}. The hydrogen consumption was monitored by a TCD detector.

In situ XRD experiments were performed on a PANalytical X'Pert Pro MPD diffractometer equipped with an Anton Paar XRK900 reaction chamber and a Cu Kα radiation source (λ = 1.54056 Å) at Oak Ridge National Laboratory, US. Approximately 0.1 g powder sample was loaded into the reaction chamber and exposed to 4 vol-% H_2/He flow. XRD patterns were recorded at a selected temperature in the 2θ range of 5°–90° at a scanning speed of 4°·min^{-1} before ramping at 10°C·min^{-1} to another temperature point. Phase identification was performed by comparison with the X-ray spectrum cards from the Joint Committee on Powder Diffraction Standards.

In situ DRIFTs experiments of CO adsorption were performed on a Nicolet Nexus 670 infrared spectrometer with a liquid N_2 cooled MCT detector and an *in situ* chamber (HC-900, Pike Technologies). DRIFT spectra were collected with 64 scans at 4 cm^{-1} resolution. Before CO adsorption, the reduction was conducted in H_2 at a desired temperature for 60 min. After reduction, the sample was cooled down to room temperature in argon and maintained for 20 min. Subsequently, a background spectrum was collected. The sample was then exposed to 1 vol-% CO/He for 30 min followed by a flow of pure He

to purge the sample surface for 20 min. After that, the spectra were collected.

Aberration-corrected STEM imaging was performed using a 200 kV JEOL 2200FS instrument fitted with a CEOS aberration corrector. Before the measurement, particle samples were ground to a powder to less than 300 mesh followed by reduction. The reduced samples were sonicated in ethanol and dropped onto lacey carbon-coated copper grids. The preparation and transfer processes were protected in UHP N_2. The JEOL 2200FS was equipped with a Bruker X-flash silicon drift detector energy dispersive X-ray (EDS) system with a 30 mm^2 active area.

Thermogravimetric (TG) and differential thermogravimetric (DTG) analysis for samples were measured by a TA high-resolution TG analyzer (series Q500). Typically, about 8 mg sample was loaded into a platinum pan in the furnace of TG instrument followed by heating from 30°C to 1000°C at a rate of 10°C·min^{-1} in air with a flow rate of 90 $cm^3 \cdot min^{-1}$.

2.3 Catalyst evaluation

The selective hydrogenation of acetylene in excess ethylene over catalysts was conducted in a quartz U-tube micro-reactor (i.d., 4 mm) at 1 atmosphere, and the details have been described in the previous work [18]. Prior to the activity tests, 30 mg catalysts were reduced in hydrogen at 30 $cm^3 \cdot min^{-1}$ for 60 min at 250°C. The catalysts underwent purging by N_2 flow at 30 $cm^3 \cdot min^{-1}$ for 10 min thereafter and then were cooled down to the reaction temperature under N_2 atmosphere. During the activity tests, each reaction temperature was maintained constantly for 30 min, prior to ramping by 25°C at the rate of 10°C·min^{-1} to the next temperature point. A feed gas with 3/1/99 $H_2/C_2H_2/C_2H_4$ ratio (a mixture of UHP H_2 from Matheson and 1.00 vol-% C_2H_2 in C_2H_4 from Scott Specialty Gases) was introduced into the reactor at a space velocity of 60 000 mL·h^{-1}·g^{-1}, and all gas flows were delivered by mass flow controllers. The gas products from the micro-reactor were analyzed three times at each reaction temperature by an on-line Shimadzu GC 17A with a 30 m × 0.32 mm (i.d.) × 1.50 μm GS-CARBONPLOT capillary column and an FID detector. The calculation methods for the conversion of acetylene and the selectivity towards ethylene are listed below,

$$C_2H_2 \text{ conversion} = \frac{C_2H_2(\text{in feed}) - C_2H_2(\text{in products})}{C_2H_2(\text{in feed})} \times 100\%, \quad (1)$$

$$C_2H_4 \text{ selectivity} = \left(1 - \frac{C_2H_6(\text{in products}) - C_2H_6(\text{in feed})}{C_2H_2(\text{in feed}) - C_2H_2(\text{in products})}\right) \times 100\%. \quad (2)$$

The pretreatment and reaction conditions of catalysts for stability test are the same as that for activity tests. The only difference is that the stability of the samples was tested at a fixed temperature, 120°C.

3 Results and discussion

3.1 Metal loading analysis

Cu and Pd actual loadings of catalysts were analyzed by an AAS and the calculated Cu:Pd atomic ratios of Pd doped Cu catalysts are summarized in Table 1.

As shown in Table 1, the actual Cu loading of the ten samples, $Cu_{1.25}$-cal, $Cu_{2.5}$-cal, Cu_{12}-cal, $Cu_{1.25}$-vac, $Cu_{2.5}$-vac, Cu_{12}-vac, $P_{0.05}Cu_{0.5}$-cal, $P_{0.05}Cu_{2.5}$-cal, $Pd_{0.05}Cu_{2.5}$-

Table 1 Metal loadings and Cu:Pd ratios of as-prepared catalysts

Samples	Loading /wt-%		Atomic ratio Cu:Pd
	Cu	Pd	
$Cu_{1.25}$-cal	1.19	–	–
$Cu_{2.5}$-cal	2.33	–	–
Cu_{12}-cal	12.17	–	–
$Cu_{1.25}$-vac	1.15	–	–
$Cu_{2.5}$-vac	2.21	–	–
Cu_{12}-vac	12.08	–	–
$Pd_{0.05}$-cal	–	0.0468	–
$Pd_{0.05}Cu_{0.5}$-cal	0.46	0.0480	16.0
$Pd_{0.05}Cu_{2.5}$-cal	2.26	0.0474	79.8
$Pd_{0.05}Cu_{2.5}$-vac	2.20	0.0445	82.8
$Pd_{0.24}Cu_{12}$-vac	11.89	0.2175	91.5

vac and $Pd_{0.24}Cu_{12}$-vac are 1.19, 2.33, 12.17, 1.15, 2.21, 12.08, 0.46, 2.26, 2.20 and 11.89 wt-% respectively. Moreover, The Pd loadings of $Pd_{0.05}$-cal, $P_{0.05}Cu_{0.5}$-cal, $P_{0.05}Cu_{2.5}$-cal, $Pd_{0.05}Cu_{2.5}$-vac and $Pd_{0.24}Cu_{12}$-vac are 0.0468, 0.0480, 0.0474, 0.0445 and 0.2175 wt-% respectively. The Cu:Pd atomic ratios of $P_{0.05}Cu_{0.5}$-cal, $P_{0.05}Cu_{2.5}$-cal, $Pd_{0.05}Cu_{2.5}$-vac and $Pd_{0.24}Cu_{12}$-vac are 16.0, 79.8, 82.8 and 91.5 respectively, and are all very close to their intended values.

3.2 H_2-TPR results

To investigate whether the samples prepared by MSI method can be reduced at low temperature without going through high-temperature pre-decomposition, and to compare the reduction behaviors of the samples prepared with the two routes, CSI and MSI, eight representative samples, $Cu_{1.25}$-cal, $Cu_{2.5}$-cal, Cu_{12}-cal, $Cu_{1.25}$-vac, $Cu_{2.5}$-vac, Cu_{12}-vac, $Pd_{0.05}Cu_{2.5}$-cal and $Pd_{0.05}Cu_{2.5}$-vac, were selected to run H_2-TPR tests. The results are presented in Fig. 1.

For Cu_y-cal (y = 1.25, 2.5 and 12) (Fig. 1(a)), all the H_2-TPR profiles show a distinct main peak of hydrogen consumption, which is well in line with the report by Dou et al. [22] and is attributed to the overlapping reduction of CuO and Cu_2O. It also can be seen that the peak shifts to lower temperature with the increase of copper loading. On the other hand, for Cu_y-vac (y = 1.25, 2.5 and 12) (Fig. 1 (b)), the similar shifting trend of the main peaks is also observed. Moreover, according to the literature [23,24], copper oxide crystallite size becomes larger with the increase of its loading for supported copper catalysts. Thus, a conclusion can be drawn for all the supported Cu samples in this study that the bigger the particles of copper species are, the easier the reduction of the particles becomes. In addition, it also can be seen in Fig. 1(b) that there is a shoulder peak in the left of the main peak for each of the Cu_y-vac samples. For example, $Cu_{2.5}$-vac shows a main H_2-TPR peak at 253°C with a shoulder at 230°C (Fig. 1(b,c)).

For $Pd_{0.05}Cu_{2.5}$-cal (Fig. 1(c)), two broad H_2-TPR features are observed at 99°C and 244°C. The peak at 99°C is attributed to the reduction of PdO [5] and the other one at 244°C should be assigned to the reduction of Cu species [22]. In comparison with the reduction peak of $Cu_{2.5}$-cal at 249°C, the peak of $Pd_{0.05}Cu_{2.5}$-cal locating at

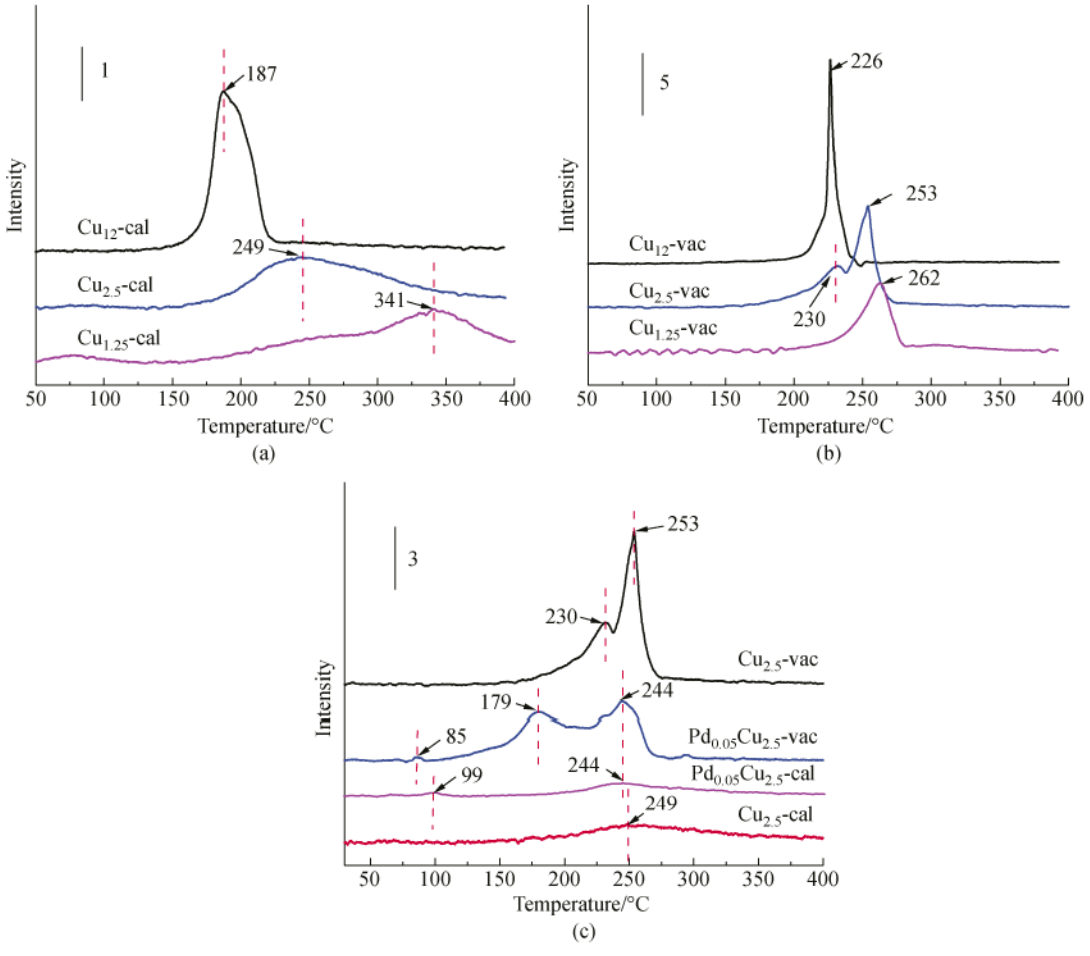

Fig. 1 H_2-TPR patterns of as prepared fresh samples

244°C shifts only by 5°C. This slight shift is in agreement with the results reported by McCue et al. [4] on a Pd doped 10% Cu catalyst (50-SI) prepared by CSI with a Cu:Pd atomic ratio of 50:1. They found that for 50-SI, the TPR peak positions for CuO reduction did not show a shift towards lower temperature suggesting that hydrogen dissociation was not easy to occur.

Further, it was speculated that almost no hydrogen dissociation was probably due to the immigration of Pd towards to the center of bimetallic particles during the reduction process. In the case of $Pd_{0.05}Cu_{2.5}$-vac, three H_2-TPR peaks at 85°C, 179°C, and 244°C are observed (Fig. 1(c)). The small peak at 85°C belongs to the reduction of Pd $(NO_3)_2$ [25], and the other two should be related to the Cu species. Notably, compared to the reduction peaks of Cu species in Cu_y-cal and $Pd_{0.05}Cu_{2.5}$-cal (in Fig. 1(a)), the two TPR peaks related to Cu species in Cu_y-vac and $Pd_{0.05}Cu_{2.5}$-vac are both much bigger and sharper, though the amount of the two samples used for the TPR tests is only about half that of Cu_y-cal and $Pd_{0.05}Cu_{2.5}$-cal. The detailed explanation will be given combing the *in situ* XRD results. In according to the literature [11,13,26], normally, there should be negative H_2-TPR peaks below 100°C for supported Pd catalysts due to the existence of Pd particles, further, the formation of palladium hydride during the reduction process. However, for both $Pd_{0.05}Cu_{2.5}$-vac and $Pd_{0.05}Cu_{2.5}$-cal, there is no negative feature at low temperature, an indication of none existence of palladium hydride during H_2 reduction. That is, almost no Pd particles and clusters exist in the two samples [11,13].

In addition, all the Cu_y-vac and Pd_xCu_y-vac samples can be completely reduced below 300°C, which suggests that the reduction of supported Cu and Pd metal salts at relatively low temperature without undergoing the high-temperature pre-decomposition process is feasible.

3.3 *In situ* XRD study

To reveal further the unique reduction processes of Cu $(NO_3)_2$ in monometallic Cu and Pd doped Cu catalysts prepared with MSI strategy, *in situ* XRD was employed in this study. However, due to the low loading of Cu in $Cu_{2.5}$-vac and $Pd_{0.05}Cu_{2.5}$-vac, the crystalline structures of Cu could not be detected during the reduction process [24,27]. Therefore, Cu_{12}-vac and $Pd_{0.24}Cu_{12}$-vac were prepared by the magnification of the nominal metal loading of $Cu_{2.5}$-vac and $Pd_{0.05}Cu_{2.5}$-vac in equal atomic proportion and used for the tests, and the results are presented in Fig. 2.

As shown in Fig. 2(a), the three broad distinct reflections at $2\theta = 37.2°$, 46.1° and 66.9° in all cases are attributed to (311), (400) and (440) facets of γ-Al_2O_3 support [28]. The XRD patterns of Cu_{12}-vac at 150°C and 175°C are almost the same, suggesting no reduction or decomposition of Cu nitrate species at the two temperatures. When the temperature increases to 200°C, the diffraction peaks at 2θ of 12.8° and 25.7° assigned to $Cu(NO_3)_2 \cdot 2.5H_2O$ become smaller and the peaks at 2θ of 32°, 33.5°, 34°, 36.2°, 40.5°, 42.2° and 43.2° attributed to $Cu_2(OH)_3(NO_3)_2$ disappearance [27]. Moreover, at this temperature, two peaks at 2θ of 35.6° and 38.7° assigned to CuO appearance, indicating the decomposition of Cu nitrate to CuO [27]. Subsequently, when the temperature reaches 225°C, two sharp peaks at 2θ of 43.3° and 50.4° appear, which are characteristic of copper metal phase [27]. Based on above phenomena, a conclusion can be drawn that the reduction of supported copper(II) nitrate on γ-Al_2O_3 follows the steps of $Cu(NO_3)_2 \rightarrow CuO \rightarrow Cu$, which is in line with the reduction steps of unsupported copper(II) nitrate [27]. Additionally, as shown in Figs. 1(a, b), H_2-TPR peaks of Cu_y-vac are much bigger and sharper than that of Cu_y-cal. Therefore, it can be concluded that the

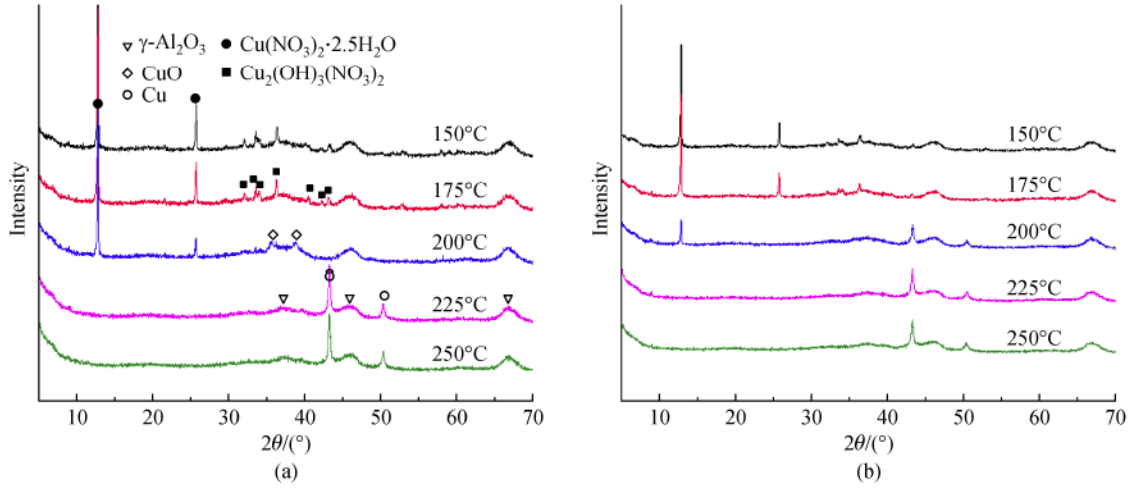

Fig. 2 (a) *In situ* XRD profiles of Cu_{12}-vac and (b) $Pd_{0.24}Cu_{12}$-vac in 4 vol-% H_2/He flow at different temperatures

H_2-TPR peaks of Cu_y-vac comprise overlapping peaks of the decomposition of $Cu(NO_3)_2$ and the reduction of CuO. The former has a great majority of contributions, and the decomposition occurred throughout the whole reduction process. Moreover, combing Fig. 1 and Fig. 2, the shoulder H_2-TPR peak of Cu_y-vac at a lower temperature should be mainly related to the decomposition of bigger $Cu(NO_3)_2$ crystals, and the main peak at higher temperature should be mainly related to the decomposition of smaller $Cu(NO_3)_2$ crystals.

On the other hand, for $Pd_{0.24}Cu_{12}$-vac (Fig. 2(b)), as temperature increases the diffraction peaks belonging to supported copper nitrate gradually decrease and the peaks ascribed to Cu metal appear. Interestingly, no CuO or Pd peaks are detected during this process. No Pd peaks detected are likely due to its low loading below the detection limit. The absence of CuO peaks suggests that the supported copper nitrate in $Pd_{0.24}Cu_{12}$-vac could be directly reduced to Cu^0 in the presence of Pd in one step, without undergoing the decomposition to CuO. This reveals that due to the presence of Pd, the reduction pathway of supported $Cu(NO_3)_2$ in the catalysts prepared by MSI is quite different from that of the Cu_y-vac catalysts. Correspondingly, the H_2-TPR peaks at 179°C and 244°C for $Pd_{0.05}Cu_{2.5}$-vac (Fig. 1(c)) should be assigned to the direct reduction of big copper nitrate crystals and highly dispersed copper nitrate to Cu metal, respectively.

Note that, for $Pd_{0.24}Cu_{12}$-vac (Fig. 2(b)), the diffraction peaks belonging to Cu metal appear at 200°C, whilst, in the case of Cu_{12}-vac, at this temperature, only $Cu(NO_3)_2$ and CuO phases can be detected. Moreover, as shown in Fig. 1(c) in Section 3.2 H_2-TPR results, with the presence of Pd, the two peaks of $Pd_{0.05}Cu_{2.5}$-vac related to Cu species shift to lower temperatures in comparison to $Cu_{2.5}$-vac. Especially, the peak at 179°C significantly shifts by 51°C in comparison to the peak of $Cu_{2.5}$-vac at 230°C. This manifests that unlike $Pd_{0.05}Cu_{2.5}$-cal, hydrogen spillover much more easily occurs from Pd to Cu species on Pd_xCu_y-vac during the reduction process.

3.4 CO *in situ* DRIFTs study

To explore the surface structure of Pd doped Cu catalysts, CO adsorption behavior of $Cu_{2.5}$-vac, $Pd_{0.05}Cu_{2.5}$-vac, $Pd_{0.05}Cu_{2.5}$-cal and $Pd_{0.05}$-cal were investigated by DRIFTs at room temperature after *in situ* reductions at 250°C for 1 h. The results are represented in Fig. 3.

Over the $Cu_{2.5}$-vac, three infrared absorption bands are observed. The strong IR band at 2107 cm^{-1} is ascribed to linear adsorbed CO species on imperfect Cu^0 sites, such as step and edge sites, as reported by Liu et al. [19] and Chen et al. [29]. It has been generalized by Dulaurent et al. [30] that IR bands above 2140 cm^{-1} were usually assigned to linear CO species on Cu^{2+} species. Therefore, the very small but broad band at around 2210 cm^{-1} indicates partial residue of Cu^{2+} ions. The band centered at ca. 1965 cm^{-1} is

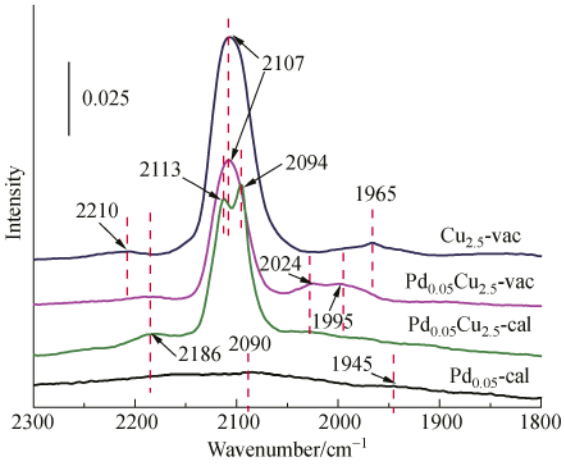

Fig. 3 CO-DRIFTs spectra of reduced samples, $Cu_{2.5}$-vac, $Pd_{0.05}Cu_{2.5}$-vac, $Pd_{0.05}Cu_{2.5}$-cal and $Pd_{0.05}$-cal

rarely mentioned in the literature. This is presumably due to the unique and mild preparation process for $Cu_{2.5}$-vac. It was found that a similar peak located at 1943 cm^{-1} has been reported by Dulaurent et al. [30], and was also not given an exact attribution. Whatever, we speculate that it should be attributed to the adsorption of CO on some kind of Cu^0 sites. In the case of $Pd_{0.05}$-cal, broad and small bands around at 2090 and 1945 cm^{-1} are observed. As reported by McCue et al. [4] and Liu et al. [19], the peak around at 2090 cm^{-1} should be assigned to CO linearly adsorbed on Pd atoms, and the peak at *ca.* 1945 cm^{-1} is related to bridge bonded CO, which suggests that the existence of Pd clusters and/or particles on $Pd_{0.05}$-cal.

Compared to $Cu_{2.5}$-vac, the FT-IR spectra collected for $Pd_{0.05}Cu_{2.5}$-vac also exhibit two bands at 2107 and around 2200 cm^{-1} related to adsorbed CO species on imperfect Cu^0 sites and Cu^{2+} species. Nevertheless, the peak at around 2200 cm^{-1} is smaller, indicating the presence of Pd is in favor of the reduction of Cu species, which is in line with the TPR and *in situ* XRD results. Besides, two broad and partially overlapped bands at ca. 1995 and 2024 cm^{-1} are distinctly observed. Haller and co-workers [31] have described the FTIR of CO on Pd-Cu with well-defined ratios in detail, and the bands at 1990 and 2031 cm^{-1} were assigned to CO adsorbed in 2-bridging configurations on Pd and CO on Cu, respectively. In our case, however, for $Pd_{0.05}$-vac (not shown in Fig. 3), $Pd_{0.05}$-cal and $Cu_{2.5}$-vac, no so obvious IR band is observed in the corresponding wavenumber range, maybe due to the much smaller metal loadings and different sample preparation method compared to Haller's work. Liu and co-workers [19] have prepared two PdCu bimetallic catalysts, I-PdCu/MgAl-cHT, and Mco-PdCu/MgAl-cHT and characterized them by FTIR of CO adsorption. A peak at about 1963 cm^{-1} was attributed to compressed-bridge CO adsorption on PdCu nanoalloys, and a band at 2071 cm^{-1} was assigned to linearly bonded CO on either PdCu alloys or Cu sites.

Besides, Pd-Cu/$ZnAl_2O_4$ catalyst has been prepared by Mierczynski et al. [32] for hydrogen production. It was found that the band located between 2095 and 1950 cm^{-1} did not overlap with the bands related to the CO species adsorbed on Pd^0 and Cu^0. It was suggested that this band did not come from any CO surface species adsorbed on Cu^0 and Pd^0, but from adsorbed CO species on PdCu alloy compound. In our case, the two broad and partially overlapped bands at ca. 1995 and 2024 cm^{-1} also do not overlap with the bands ascribed to the adsorbed CO species on any metal species in $Cu_{2.5}$-vac and $Pd_{0.05}$-cal catalysts. Therefore, the two peaks should belong to the CO species adsorbed on PdCu alloys.

For $Pd_{0.05}Cu_{2.5}$-cal, two big and sharp peaks at about 2113 and 2094 cm^{-1} are exhibited. As reported by Liu et al. [19] and Chen et al. [29], the peak at 2113 cm^{-1} is attributed to CO adsorbed linearly on the step and edge sites of Cu^0 particles, and the peak at 2094 cm^{-1} is due to CO adsorbed on low-index planes, such as the (111) and (100) facets of Cu metal. It indicates that due to the calcination step of CSI, the crystallinity of Cu^0 in $Pd_{0.05}Cu_{2.5}$-cal is higher than that in $Cu_{2.5}$-vac and $Pd_{0.05}Cu_{2.5}$-vac. However, no pronounced peak is below 2094 cm^{-1}, indicating almost no formation of PdCu alloy and no existence of Pd clusters and/or particles on the surface of $Pd_{0.05}Cu_{2.5}$-cal [4,19,30].

In brief, based on the CO *in situ* DRIFTs study, it can be inferred that Cu particles in Pd_xCu_y-cal prepared by CSI possess higher crystallinity and more exposed low-index planes, which should be attributed to the calcination step during sample preparation. Combing with the TPR results, Pd should be rare on the surface of Cu particles, as a result of the facile migration of Pd below the surface layer of Cu [4,33]. In comparison, for Pd_xCu_y-vac prepared by MSI, there's a certain amount of PdCu alloys on the surface of metal particles, which is likely due to the room temperature-vacuum drying and the direct reduction without pre-calcination.

3.5 STEM characterization

To gain more information about the morphology of Pd doped Cu catalysts prepared with the two different methodologies in this study, (HAADF) STEM images of $Cu_{2.5}$-vac, $Pd_{0.05}Cu_{2.5}$-cal and $Pd_{0.05}Cu_{2.5}$-vac and the EDS data of $Pd_{0.05}Cu_{2.5}$-vac were acquired after reduction and shown in Fig. 4.

Notably, during the STEM scanning process, it was strenuous to find a metal particle on all the three samples. Moreover, the detected metal particles are all about 5 nm or less (not shown here). This indicates that all the tested samples possess much high metal dispersion. In addition, no Pd particles are found in the two PdCu bimetallic catalysts, which is in line well with TPR and CO *in situ* DRIFTs results as shown in Fig. 1(c) and Fig. 3.

For $Cu_{2.5}$-vac, as shown in Figs. 4(a,d), the particle has a lattice spacing value of 0.209 nm, which is consistent with the (111) planes of Cu [19]. In the case of $Pd_{0.05}Cu_{2.5}$-cal and $Pd_{0.05}Cu_{2.5}$-vac, the lattice fringes throughout the particles in Figs. 4(b,e, and c,f) are around 0.218 nm which is the characteristic of PdCu alloy (111) [19]. For $Pd_{0.05}Cu_{2.5}$-vac, the result is in line with that of CO *in situ* DRIFTs test. On the other hand, for $Pd_{0.05}Cu_{2.5}$-cal, the result suggests that except for the facile migration below the surface layer of Cu, Pd also tends to form PdCu alloy there. In addition, EDS elemental maps of a randomly selected particle in $Pd_{0.05}Cu_{2.5}$-vac are shown in Figs. 4(g–i). The three images exhibit the existence of both Cu and Pd elements and the uniform distribution throughout the nanoparticle. This demonstrates again that the MSI method can form Pd highly dispersed PdCu bimetallic catalysts.

3.6 Catalytic performance tests

Figure 5 summarizes the results of acetylene conversion and ethylene selectivity over the four representative samples $Pd_{0.05}$-cal, $Pd_{0.05}Cu_{0.5}$-cal, $Pd_{0.05}Cu_{2.5}$-cal and $Pd_{0.05}Cu_{2.5}$-vac.

As shown in Fig. 5(a), the conversion of acetylene over all samples increases with the increase of temperature with the conversion activity of $Pd_{0.05}$-cal>$Pd_{0.05}Cu_{0.5}$-cal>$Pd_{0.05}Cu_{2.5}$-cal ≈ $Pd_{0.05}Cu_{2.5}$-vac. Although $Pd_{0.05}$-cal possesses the highest activity, high and relatively stable selectivity to ethylene over the sample only occurs when the temperature is below 75°C, and the conversion is less than 36%. After that, the selectivity decreases sharply with the temperature increase. Further, when the conversion of acetylene reaches 100% at 100°C, the corresponding selectivity to ethylene is even as low as –14.6% (Figs. 5(b,c)). This should be due to the existence of Pd particles and clusters on $Pd_{0.05}$-cal [4], which have been proved by FTIR results shown in Fig. 4(b). Compared with $Pd_{0.05}$-cal, the selectivity over $Pd_{0.05}Cu_{0.5}$-cal is dramatically improved, even though the selectivity begins to drop off significantly from 100°C with the increase of temperature, it is still up to 51.8% when the acetylene conversion reaches 100% at 120°C (Figs. 5(b,c)). This indicates that the addition of copper is enormously effective for the selectivity to ethylene even the Cu loading is only 0.46 wt-%. Moreover, it also can be seen from Figs. 5(b,c) that with the copper loading increasing to 2.26 wt-%, the selectivity towards ethylene reaches up to 81.8% at 100% acetylene conversion. However, $Pd_{0.05}Cu_{2.5}$-vac displays slightly less selectivity to ethylene in the tested temperature range (Figs. 5(b,c)) compared with $Pd_{0.05}Cu_{2.5}$-cal. The phenomenon also appears in the following stability test. This should be attributed to the relatively easy surface enrichment of Pd in Cu particles in $Pd_{0.05}Cu_{2.5}$-vac compared with $Pd_{0.05}Cu_{2.5}$-cal, due to their different preparation methods as discussed in Section 3.4 CO *in situ* DRIFTs study.

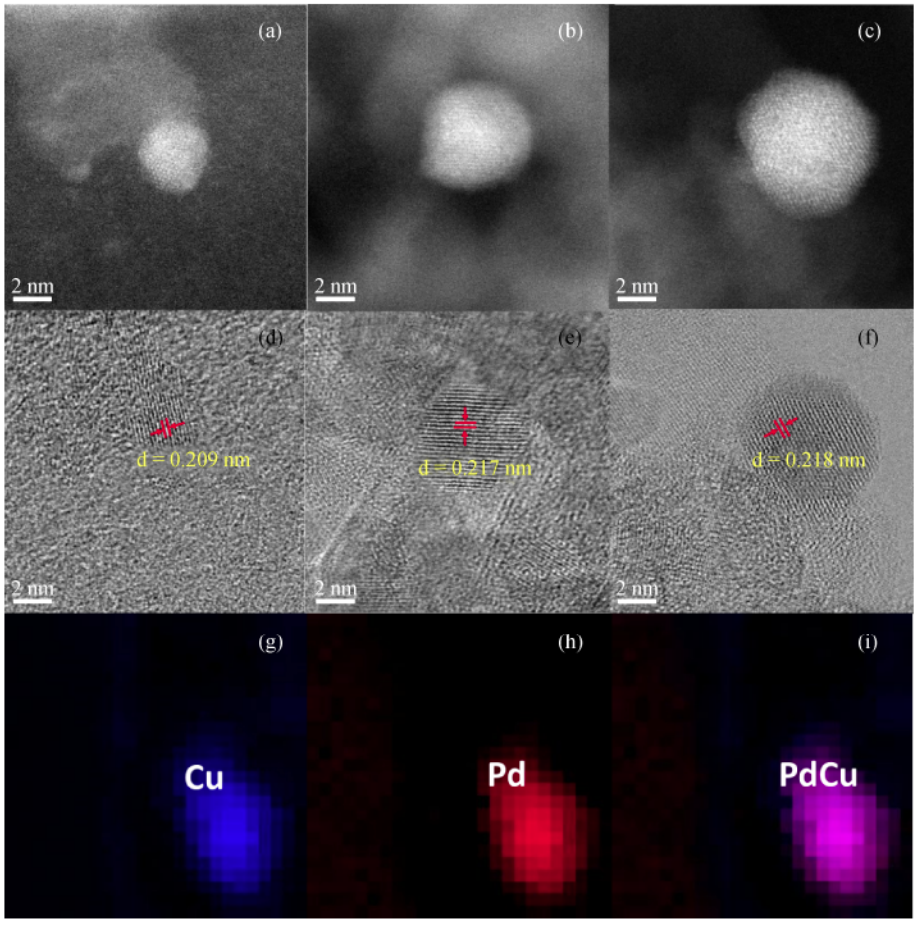

Fig. 4 High-angle annular dark field (HAADF) STEM images of (a) $Cu_{2.5}$-vac, (b) $Pd_{0.05}Cu_{2.5}$-cal and (c) $Pd_{0.05}Cu_{2.5}$-vac and their corresponding lattice fringe (d), (e) and (f), respectively; STEM–EDS elemental maps (g, h and i) of a random particle in $Pd_{0.05}Cu_{2.5}$-vac

The stability of the catalysts is very important for their industrial applications. Herein, we tested the stability of $Pd_{0.05}Cu_{2.5}$-cal and $Pd_{0.05}Cu_{2.5}$-vac at 120°C. As shown in Fig. 6(a), after reaction for 12 h, the acetylene conversion over $Pd_{0.05}Cu_{2.5}$-cal falls to 47.7% from 71.9%, and the selectivity to ethylene over this sample decreases from 97.0% to 92.5% (Fig. 6(b)). By contrast, for $Pd_{0.05}Cu_{2.5}$-vac, the conversion and selectivity are both more stable. For the 12-h test, the conversion over $Pd_{0.05}Cu_{2.5}$-vac decreases slightly from 73.3% to 65.2%, and the selectivity only less than two percent decrease from 93.4% to 91.8% (Fig. 6(a,b)). These indicate that PdCu bimetallic catalyst prepared by MSI in this study possesses preferable stability. One possible explanation for the preferable stability of $Pd_{0.05}Cu_{2.5}$-vac is its structural stability. As reported by Marakatti et al. [34] and Shao et al. [35], structural stability is a property of intermetallic compounds. Thus this kind of compounds could maintain their surface structure well under reaction conditions. Besides, carbonaceous deposits on catalyst surface during a reaction is another factor affecting the stability of catalysts. To obtain information about the formation of carbonaceous deposits on the catalyst surface during the stability tests, TG-DTG analysis in an air atmosphere for reduced $Pd_{0.05}Cu_{2.5}$-cal and $Pd_{0.05}Cu_{2.5}$-vac before and after aging experiment were conducted. The results are shown in Fig. 7.

The weight loss before 120°C can be attributed to the loss of physically absorbed water. To get the relatively accurate amount of carbonaceous deposits formed on $Pd_{0.05}Cu_{2.5}$-cal and $Pd_{0.05}Cu_{2.5}$-vac, the weight loss ascribed to the oxidation or decomposition of carbonaceous was computed more scientifically. That is the weight loss of used sample subtracting the weight loss of the corresponding reduced sample in the temperature range of 120°C–1000°C. In this way, the weight losses belonging to carbonaceous deposits over $Pd_{0.05}Cu_{2.5}$-cal and $Pd_{0.05}Cu_{2.5}$-vac are 9.25% and 7.12% respectively. The slightly smaller amount of carbonaceous deposits on the used $Pd_{0.05}Cu_{2.5}$-vac indicates better resistibility against carbon deposition [19].

DTG results of the used $Pd_{0.05}Cu_{2.5}$-cal and $Pd_{0.05}Cu_{2.5}$-vac comprises the main peak at about 290°C and a shoulder near 360°C. The peak at around 290°C is

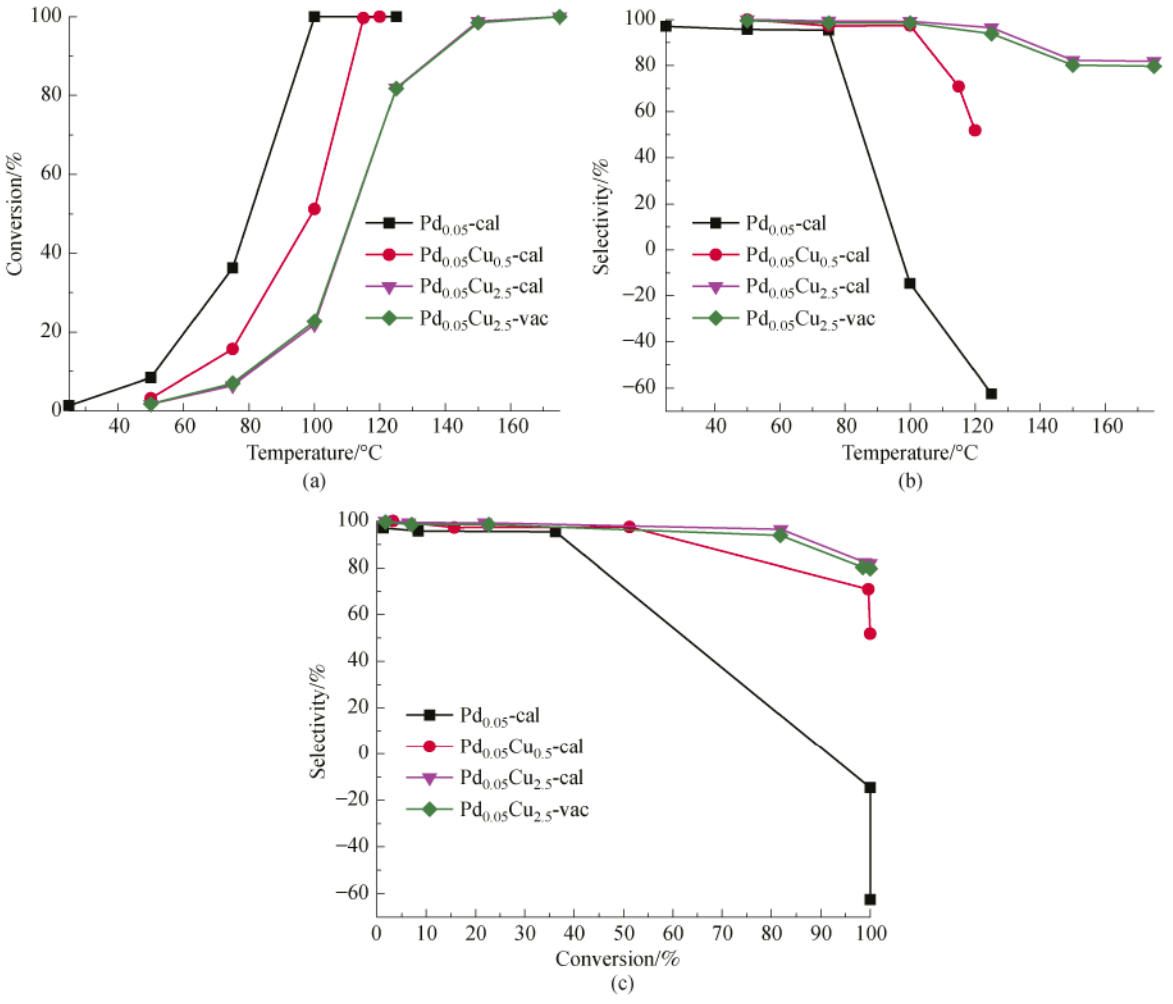

Fig. 5 (a) Acetylene conversion and (b) selectivity to ethylene versus reaction temperature and the selectivity vs. the conversion over $Pd_{0.05}$-cal, $Pd_{0.05}Cu_{0.5}$-cal, $Pd_{0.05}Cu_{2.5}$-cal and $Pd_{0.05}Cu_{2.5}$-vac. H_2:C_2H_2:C_2H_4 = 3:1:99, GHSV = 60000 cc·g^{-1}·h^{-1}

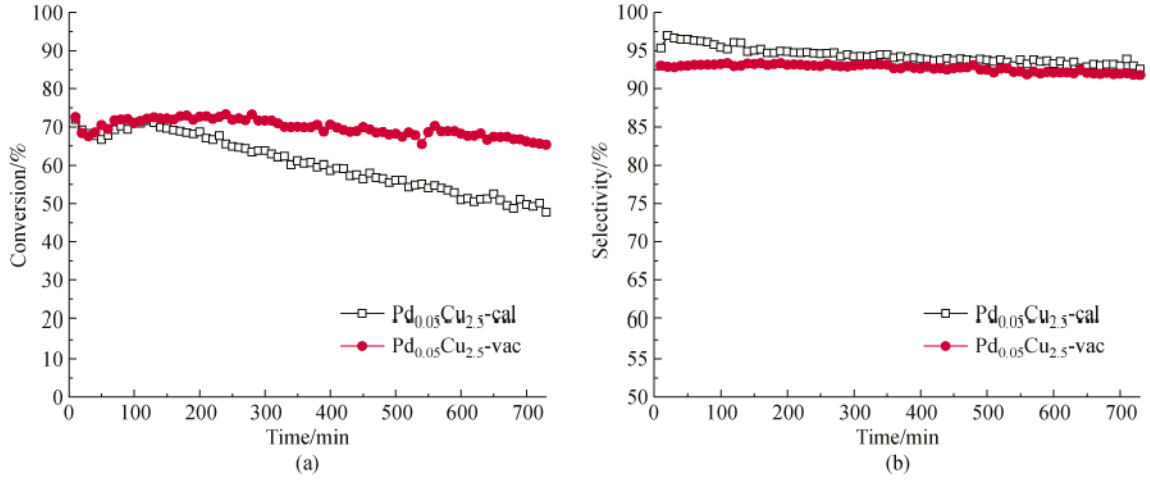

Fig. 6 (a) Acetylene conversion and (b) selectivity to ethylene versus reaction time over $Pd_{0.05}Cu_{2.5}$-cal and $Pd_{0.05}Cu_{2.5}$-vac. H_2:C_2H_2:C_2H_4 = 3:1:99, GHSV = 60000 cc·g^{-1}·h^{-1}, reaction temperature: 120°C

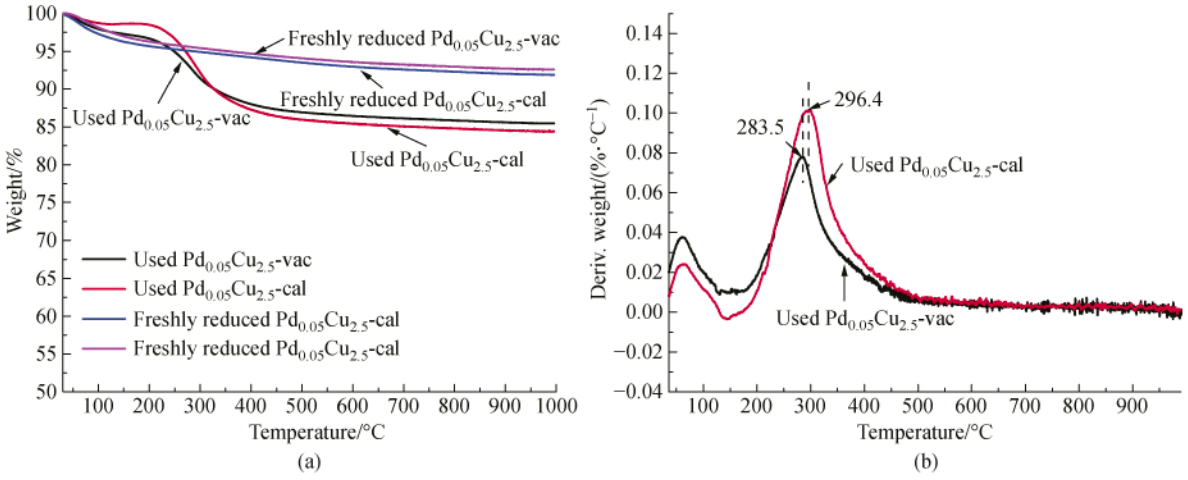

Fig. 7 (a) TG results of fresh and used $Pd_{0.05}Cu_{2.5}$-cal and $Pd_{0.05}Cu_{2.5}$-vac and (b) corresponding DTG results of the two used samples derived from TG

associated with the combustion of coke deposited on metal sites or/and hydrocarbons traped on surface or pores of the catalysts, which does not affect the reaction [19,36]. The shoulder at about 360°C is attributed to the combustion of amorphous coke. It reduces the availability of hydrogen and/or acetylene [19]. The DTG peak of the used $Pd_{0.05}Cu_{2.5}$-vac shifts to lower temperature and the peak area becomes smaller compared with that of the used $Pd_{0.05}Cu_{2.5}$-cal, also indicating the better resistance against the deposition of the carbonaceous compound and thus superior stability. Monometallic copper is traditionally regarded as poor partial hydrogenation catalyst because of easy oligomer formation [37]. On the other hand, for PdCu bimetallic catalysts, the dilution of Pd by Cu and synergistic interaction of Cu and Pd have already been proved to effectively improve the anti-carbon deposition properity [4,17,18,33]. Therefore, it is speculated that the difference of resistance against the deposition of the carbonaceous compound between $Pd_{0.05}Cu_{2.5}$-cal and $Pd_{0.05}Cu_{2.5}$-vac should be due to the differences of their surface species and surface structure.

4 Conclusions

CSI and MSI methods have been employed to prepare Pd doped Cu catalysts with low metal loading for selective hydrogenation of acetylene in ethylene. TGA-DTGA, H_2-TPR, *in situ* XRD and CO *in situ* DRIFTs results suggest that the supported Cu copper (II) nitrate in the PdCu bimetallic catalysts prepared with MSI could be directly reduced to Cu metal particles. Moreover, CO *in situ* DRIFTs and STEM results indicate that with MSI, Pd can form PdCu alloys on the surface of metal particles, whereas, with CSI, Pd tends to migrate and exist below the surface layer of Cu. Compared with CSI, MSI was proved to be a feasible method to prepare PdCu bimetallic catalysts with preferable stability, due to structure stability and better resistance against the deposition of coke. Moreover, for the samples prepared by CSI, the effects of Cu loadings, Cu:Pd atomic ratios and preparation methods on the performance of catalysts have been discussed. When the acetylene conversion reaches 100%, the corresponding selectivity to ethylene over $Pd_{0.05}$-cal is −14.6%, however, the selectivity over $Pd_{0.05}Cu_{0.5}$-cal is up to 51.8%, though the addition of Cu is only 0.46 wt-%. Further, keeping Pd loading around 0.05 wt-%, the selectivity to ethylene can be dramatically improved with the increase of Cu loading. For example, when the loading of Cu increases to 2.26 wt-%, the selectivity increases to 81.8% at 100% acetylene conversion. Moreover, this work provides a reference to design ultralow-metal-loading PdCu bimetallic catalysts with high performance, especially preferable stability for selective hydrogenation of acetylene.

Acknowledgements The financial support of the National Natural Science Foundation of China (Grant No. 1263094), Welch Foundation (No. T-0014), Key Scientific and Technological Project of Henan province, China (No. 182102410072) and Shanxi International Cooperation Project (No. 201703D421037) are acknowledged. A portion of this research was conducted at the Center for Nanophase Materials Sciences, which is a DOE Office of Science User Facility.

References

1. Vignola E, Steinmann S N, Farra A A, Vandegehuchte B D, Curulla D, Sautet P. Evaluating the risk of C–C bond formation during selective hydrogenation of acetylene on palladium. ACS Catalysis, 2018, 8(3): 1662–1671
2. Hu M, Zhang J, Zhu W, Chen Z, Gao X, Du X, Wan J, Zhou K,

Chen C, Li Y. 50 ppm of Pd dispersed on $Ni(OH)_2$ nanosheets catalyzing semi-hydrogenation of acetylene with high activity and selectivity. Nano Research, 2018, 11(2): 905–912

3. Pei G X, Liu X, Yang X, Zhang L, Wang A, Li L, Wang H, Wang X, Zhang T. Performance of Cu-alloyed Pd single-atom catalyst for semihydrogenation of acetylene under simulated front-end conditions. ACS Catalysis, 2017, 7(2): 1491–1500
4. McCue A J, Shepherd A M, Anderson J A. Optimisation of preparation method for Pd doped Cu/Al_2O_3 catalysts for selective acetylene hydrogenation. Catalysis Science & Technology, 2015, 5 (5): 2880–2890
5. McCue A J, Baker R T, Anderson J A. Acetylene hydrogenation over structured Au-Pd catalysts. Faraday Discussions, 2016, 188: 499–523
6. Feng J, Liu Y, Yin M, He Y, Zhao J, Sun J, Li D. Preparation and structure-property relationships of supported trimetallic PdAuAg catalysts for the selective hydrogenation of acetylene. Journal of Catalysis, 2016, 344: 854–864
7. Liu Y, Zhao J, He Y, Feng J, Wu T, Li D. Highly efficient PdAg catalyst using a reducible Mg-Ti mixed oxide for selective hydrogenation of acetylene: Role of acidic and basic sites. Journal of Catalysis, 2017, 348: 135–145
8. Zhou H, Yang X, Li L, Liu X, Huang Y, Pan X, Wang A, Li J, Zhang T. PdZn intermetallic nanostructure with Pd-Zn-Pd ensembles for highly active and chemoselective semi-hydrogenation of acetylene. ACS Catalysis, 2016, 6(2): 1054–1061
9. Meuniera F, Maffrea M, Schuurmana Y, Colussib S, Trovarelli A. Acetylene semi-hydrogenation over $Pd\text{-}Zn/CeO_2$: Relevance of CO adsorption and methanation as descriptors of selectivity. Catalysis Communications, 2018, 105: 52–55
10. Kruppe C M, Krooswyk J D, Trenary M. Selective hydrogenation of acetylene to ethylene in the presence of a carbonaceous surface layer on a Pd/Cu (111) single-atom alloy. ACS Catalysis, 2017, 7(12): 8042–8049
11. McCue A J, Guerrero-Ruiz A, Rodríguez-Ramos I, Anderson J A. Palladium sulphide—a highly selective catalyst for the gas phase hydrogenation of alkynes to alkenes. Journal of Catalysis, 2016, 340: 10–16
12. Hu M, Wang X. Effect of N_3–species on selective acetylene hydrogenation over Pd/SAC catalysts. Catalysis Today, 2016, 263: 98–104
13. McCue A J, McKenna F M, Anderson J A. Triphenylphosphine: A ligand for heterogeneous catalysis too? Selectivity enhancement in acetylene hydrogenation over modified Pd/TiO_2 catalyst. Catalysis Science & Technology, 2015, 5(4): 2449–2459
14. Kyriakou G, Boucher M B, Jewell A D, Lewis E A, Lawton T J, Baber A E, Tierney H L, Flytzani-Stephanopoulos M, Sykes E C H. Isolated metal atom geometries as a strategy for selective heterogeneous hydrogenations. Science, 2012, 335(6073): 1209–1212
15. Cao X, Ji Y, Luo Y. Dehydrogenation of propane to propylene by a Pd/Cu single-atom catalyst: Insight from first-principles calculations. Journal of Physical Chemistry C, 2015, 119(2): 1016–1023
16. Cao X, Fu Q, Luo Y. Catalytic activity of Pd-doped Cu nanoparticles for hydrogenation as a single-atom-alloy catalyst. Physical Chemistry Chemical Physics, 2014, 16(18): 8367–8375
17. Boucher M B, Zugic B, Cladaras G, Kammert J, Marcinkowski M D, Lawton T J, Sykes E C H, Flytzani-Stephanopoulos M. Single atom alloy surface analogs in $Pd_{0.18}Cu_{15}$ nanoparticles for selective hydrogenation reactions. Physical Chemistry Chemical Physics, 2013, 15(29): 12187–12196
18. Cao X, Mirjalili A, Wheeler J, Xie W, Jang B W L. Investigation of the preparation methodologies of Pd-Cu single atom alloy catalysts for selective hydrogenation of acetylene. Frontiers of Chemical Science & Engineering, 2015, 9(4): 442–449
19. Liu Y, He Y, Zhou D, Feng J, Li D. Catalytic performance of Pd-promoted Cu hydrotalcite-derived catalysts in partial hydrogenation of acetylene: Effect of Pd-Cu alloy formation. Catalysis Science & Technology, 2016, 6(9): 3027–3037
20. Li Y N, Jang B W L. Non-thermal RF plasma effects on surface properties of Pd/TiO_2 catalysts for selective hydrogenation of acetylene. Applied Catalysis A, General, 2011, 392(1-2): 173–179
21. Liu C J, Li M, Wang J, Zhou X, Guo Q, Yan J, Li Y. Plasma methods for preparing green catalysts: Current status and perspective. Chinese Journal of Catalysis, 2016, 37(3): 340–348
22. Dow W P, Wang Y, Huang T. TPR and XRD studies of yttria-doped ceria/γ-alumina-supported copper oxide catalyst. Applied Catalysis A, General, 2000, 190(1-2): 25–34
23. Renuka N K, Shijina A V, Praveen A K, Aniz C U. Redox properties and catalytic activity of $CuO/\gamma\text{-}Al_2O_3$ Meso phase. Journal of Colloid and Interface Science, 2014, 434: 195–200
24. Sagar G V, Rao P V R, Srikanth C S, Chary K V R. Dispersion and reactivity of copper catalysts supported on $Al_2O_3\text{-}ZrO_2$. Journal of Physical Chemistry B, 2006, 110(28): 13881–13888
25. Li Y, Jang B W L. Selective hydrogenation of acetylene over Pd/Al_2O_3 catalysts: Effect of non-thermal RF plasma preparation methodologies. Topics in Catalysis, 2017, 60(12-14): 1–12
26. Sa J, Arteaga G D, Daley R A, Bernardi J, Anderson J A. Factors influencing hydride formation in a Pd/TiO_2 Catalyst. Journal of Physical Chemistry B, 2006, 110(34): 17090–17095
27. Ryu S K, Lee W K, Park S J. Thermal decomposition of hydrated copper nitrate $[Cu(NO_3)_2 \cdot 3H_2O]$ on activated carbon fibers. Carbon letters, 2004, 5: 180–185
28. Wu C, Yuan W, Huang Y, Xia Y, Yang H, Wang H, Liu X. Conversion of xylose into furfural catalyzed by bifunctional acidic ionic liquid immobilized on the surface of magnetic $\gamma\text{-}Al_2O_3$. Catalysis Letters, 2017, 147(4): 953–963
29. Chen C S, Lin J H, Lai T W. Low-temperature water gas shift reaction on Cu/SiO_2 prepared by an atomic layer epitaxy technique. Chemical Communications, 2008, 40(40): 4983–4985
30. Dulaurent O, Courtois X, Perrichon V, Bianchi D J. Heats of adsorption of CO on a Cu/Al_2O_3 catalyst using FTIR spectroscopy at high temperatures and under adsorption equilibrium conditions. Journal of Physical Chemistry B, 2000, 104(25): 6001–6011
31. Fernández-García M, Anderson J A, Haller G L. Alloy formation and stability in Pd-Cu bimetallic catalysts. Journal of Chemical Physics, 1996, 100(40): 16247–16254
32. Mierczynski P, Vasilev K, Mierczynsk A, Maniukiewicz W, Maniecki T P. Highly selective $Pd\text{-}Cu/ZnAl_2O_4$ catalyst for hydrogen production. Applied Catalysis A, General, 2014, 479(6): 26–34
33. McCue A J, Anderson J A. CO induced surface segregation as a

means of improving surface composition and enhancing performance of CuPd bimetallic catalysts. Journal of Catalysis, 2016, 344: 854–864

34. Marakatti V S, Sarma S C, Joseph B, Banerjee D, Peter S C. Synthetically tuned atomic ordering in PdCu nanoparticles with enhanced catalytic activity towards solvent free benzylamine oxidation. ACS Applied Materials & Interfaces, 2017, 9(4): 3602–3615
35. Shao L D, Zhang W, Armbruster M, Teschner D, Girgsdies F, Zhang B S, Timpe O, Friedrich M, Schlogl R, Su D S. Nanosizing intermetallic compounds onto carbon nanotubes: Active and selective hydrogenation catalysts. Angewandte Chemie International Edition, 2011, 50(43): 10231–10235
36. Zhang S, Chen C Y, Jang B W L, Zhu A M. Radio-frequency H_2 plasma treatment of AuPd/TiO_2 catalyst for selective hydrogenation of acetylene in excess ethylene. Catalysis Today, 2015, 256: 161–169
37. Lee J W, Liu X, Mou C Y. Selective hydrogenation of acetylene over SBA-15 supported Au-Cu bimetallic catalysts. Journal of the Chinese Chemical Society (Taipei), 2013, 60(7): 907–914